# Next-Generation Sequencing Reveals Differential Responses to Acute versus Long-Term Exposures to Graphene Oxide in Human Lung Cells

**Article** *in* Small · March 2020

DOI: 10.1002/smll.201907686



**7 authors**, including:

Sourav Prasanna Mukherjee
Karolinska Institutet
**25** PUBLICATIONS **705** CITATIONS
SEE PROFILE

Govind Sharan Gupta
Karolinska Institutet
**16** PUBLICATIONS **138** CITATIONS
SEE PROFILE

Katharina Klöditz
Karolinska Institutet
**10** PUBLICATIONS **74** CITATIONS
SEE PROFILE

Artur Filipe Rodrigues
University of Coimbra
**24** PUBLICATIONS **250** CITATIONS
SEE PROFILE

NANO · MICRO small
www.small-journal.com



# Next-Generation Sequencing Reveals Differential Responses to Acute versus Long-Term Exposures to Graphene Oxide in Human Lung Cells

*Sourav P. Mukherjee, Govind Gupta, Katharina Klöditz, Jun Wang, Artur Filipe Rodrigues, Kostas Kostarelos, and Bengt Fadeel**

**Numerous studies have addressed the biological impact of graphene-based materials including graphene oxide (GO), yet few have focused on long-term effects. Here, RNA sequencing is utilized to unearth responses of human lung cells to GO. To this end, the BEAS-2B cell line derived from normal human bronchial epithelium is subjected to repeated, low-dose exposures of GO (1 or 5 μg mL$^{-1}$) for 28 days or to the equivalent, cumulative amount of GO for 48 h. Then, samples are analyzed by using the NovaSeq 6000 sequencing system followed by pathway analysis and gene ontology enrichment analysis of the differentially expressed genes. Significant differences are seen between the low-dose, long-term exposures and the high-dose, short-term exposures. Hence, exposure to GO for 48 h results in mitochondrial dysfunction. In contrast, exposure to GO for 28 days is characterized by engagement of apoptosis pathways with downregulation of genes belonging to the inhibitor of apoptosis protein (IAP) family. Validation experiments confirm that long-term exposure to GO affects the apoptosis threshold in lung cells, accompanied by a loss of IAPs. These studies reveal the sensitivity of RNA-sequencing approaches and show that acute exposure to GO is not a good predictor of the long-term effects of GO.**

## 1. Introduction

Significant progress has been made in recent years with respect to mechanism-based hazard assessment of nanomaterials.[1] Developments in so-called next-generation sequencing technologies have enabled the evaluation of the biological interactions of nanomaterials at an unprecedented level of detail.[2] RNA sequencing, which provides far more precise measurements of levels of transcripts when compared to other conventional approaches, has emerged as the favored method for gene expression profiling of cells and tissues.[3] Using RNA sequencing of primary human lung cells, we previously reported that low-dose (non-cytotoxic) exposure to cationic dendrimers caused significant changes in gene expression.[4] These changes overlapped with senescence-related gene signatures and were found to correspond to cell cycle arrest. Mitchell et al.[5] applied single-cell RNA sequencing to lung epithelial cells carrying defined loads of aminated or carboxylated quantum dots. The authors found that the genes that could distinguish between the different nanomaterial exposures were enriched in stress response and cell cycle related processes. Bornholdt et al.[6] recently cataloged alternative transcription start sites in mouse lungs following intratracheal instillation of multiwalled carbon nanotubes (MWCNTs) by using a highly sensitive RNA-sequencing-based method. Mortimer et al.[7] applied RNA sequencing to *Pseudomonas aeruginosa* exposed to carbonaceous and boron nitride nanomaterials at nongrowth-inhibitory concentrations and concluded, based on the transcriptomics results, that nanomaterials that appear relatively innocuous when assessed by conventional toxicity assays may nevertheless modulate bacterial responses. Together, these studies serve to illustrate how omics approaches can be applied in nanosafety research to study cellular and organismal responses to a range of materials.

Safe and sustainable development of graphene-enabled technologies requires that careful attention be paid to the potential impact of these materials on human health and the environment. Indeed, it is important to explore the structure–activity

Dr. S. P. Mukherjee, Dr. G. Gupta, Dr. K. Klöditz, Prof. B. Fadeel
Nanosafety and Nanomedicine Laboratory
Division of Molecular Toxicology
Institute of Environmental Medicine
Karolinska Institutet
Stockholm 171 77, Sweden
E-mail: bengt.fadeel@ki.se
Dr. J. Wang
Science for Life Laboratory
Department of Biochemistry and Biophysics
Stockholm University
Stockholm 106 91, Sweden
Dr. A. F. Rodrigues, Prof. K. Kostarelos
Nanomedicine Laboratory
Faculty of Biology
Medical and Human Sciences, and National Graphene Institute
University of Manchester
Manchester M13 9PT, UK

The ORCID identification number(s) for the author(s) of this article can be found under https://doi.org/10.1002/smll.201907686.

**DOI: 10.1002/smll.201907686**

 

relationships of graphene-based materials (GBMs).[8] Previous studies have shown that the lateral dimensions as well as the number of layers play important roles in the acute toxicity of GBMs such as graphene oxide (GO).[9–13] However, there are few if any studies in which the long-term impact is examined. Here, we addressed the impact of GO sheets with varying lateral dimensions on human lung cells by applying RNA sequencing coupled with computational analysis of the transcriptomics data. Specifically, we asked whether transcriptomics approaches could be used to distinguish short-term and long-term exposures to GO and if so, which biological processes were involved. We then applied cell-based assays in order to validate the results.

## 2. Results

### 2.1. Exposure of Human Bronchial Epithelial Cells to Graphene Oxide (GO)

The GO samples in the present study were produced by a modified Hummers' method, as previously described, and consisted of single to few-layer sheets with similar surface chemistry and thickness, but with varying lateral dimensions.[14] Large GO (GO-L) was comprised of micron-sized sheets ranging between 1 and 30 μm in lateral dimensions, whereas small GO (GO-S) consisted mainly of sheets between 50 and 2 μm in lateral dimensions. For comparison, most eukaryotic cells are between 10 and 30 μm in diameter; human alveolar macrophages are ≈20 μm in diameter. Ultrasmall GO (GO-US) was comprised of sub-micrometer sheets of 50–300 nm in lateral dimensions.[14] Table S1 (Supporting Information) provides a summary of the properties of the materials. The GO sheets displayed mild agglomeration in cell culture medium, but differences in lateral dimensions between the three materials were retained (data not shown).

The GO samples were endotoxin-free as shown by using a human macrophage-based assay.[14] The latter study also showed that the three GO samples were noncytotoxic for primary human macrophages (at doses up to 75 μg $mL^{-1}$), in line with previous work using similar, single to few-layer sheets of GO.[15] To study the impact of the GO sheets on human lung cells, we selected the BEAS-2B cell line, a nontumorigenic, SV40-transformed human lung cell line suitable for long-term culture as evidenced in several previous long-term studies of metallic and carbonaceous nanomaterials.[16–18] The BEAS-2B cell line was originally derived from normal human bronchial epithelium obtained at autopsy,[19,20] and the cells are normally maintained in serum-free, bronchial epithelial cell growth medium supplemented with specific growth factors, as detailed in the experimental section. Using these cells, we performed acute versus long-term exposures to equivalent doses of GO (refer to the schematic diagram in **Figure 1**a). Hence, we exposed BEAS-2B cells to 1 or 5 μg $mL^{-1}$ twice per week for up to 4 weeks (in other words, a total dose of 8 and 40 μg $mL^{-1}$, respectively). In addition, we exposed the cells to the same, cumulative dose (8 and 40 μg $mL^{-1}$) for 48 h. Cells were also exposed to a high dose (80 μg $mL^{-1}$) for 48 h, for comparison. Cells were harvested at 48 h and at 1 week and 4 weeks, respectively, and samples were submitted for RNA sequencing, as detailed below. Following analysis of the transcriptomics data, we repeated the short-term and long-term exposures (up to 4 weeks), in order to perform biological validation experiments on an independent set of samples.

### 2.2. Transcriptomics-Based Assessment upon Acute Exposure to GO

BEAS-2B cells were exposed to the three different GO materials (GO-US, GO-S, and GO-L) for 48 h and no cytotoxicity was observed, as evidenced by using the Alamar blue assay (Figure 1b). Cells were then exposed to GO at the indicated concentrations and samples were harvested for isolation of total RNA by using standard methods.[4] The quality of the RNA was assessed and samples with RIN values above 8 were subjected to RNA sequencing using the Illumina NovaSeq 6000 sequencing platform. The RNA sequencing generated ≈1 TB of raw sequence data, yielding a sequencing depth of >20 million reads per sample. More than 88% of the obtained reads could be mapped to the annotated human genome (GRCh37). Data normalization was carried out in conjunction with the count-based differential expression analysis using R/Bioconductor.[21] Differential tag abundance using counts of genes, filtered to include only tags with an abundance of >1 count per million (cpm), was determined using the R/Bioconductor package edgeR and the negative binomial model.[22] Bioinformatics processing of the RNA sequencing data was performed in R wherein each GO exposure was compared with cells cultured in medium alone and here the transcript length was also normalized for unbiased evaluation of differential gene expression. After initial statistical processing, further bioinformatics analyses were performed by using the ingenuity pathway analysis (IPA) tool,[23] and database for annotation, visualization and integrated discovery (DAVID),[24] as indicated in the following sections.

#### *2.2.1. Differential Gene Expression Analysis*

RNA sequencing showed that significant numbers of differentially expressed genes (DEGs) were affected by all three materials (Table S2, Supporting Information). Only genes with *p*-values lower than 0.05 after FDR correction for multiple testing were included. Volcano plots displaying gene expression changes in BEAS-2B cells exposed for 48 h to GO-US, GO-S, and GO-L are shown in Figure S1 (Supporting Information). Venn diagrams were plotted for the upregulated (**Figure 2**a) and downregulated (Figure 2b) DEGs at 48 h versus day 28 (discussed below) to illustrate the degree of overlap between the samples (with a cut-off for FDR adjusted *p*-values of 0.05 for all the DEGs). The analysis clearly demonstrated that there is little overlap between DEGs at 48 h and 28 days.

#### *2.2.2. Canonical Pathway Enrichment Analysis*

IPA was used in order to further interpret the RNA-sequencing data by performing canonical pathway enrichment analysis.

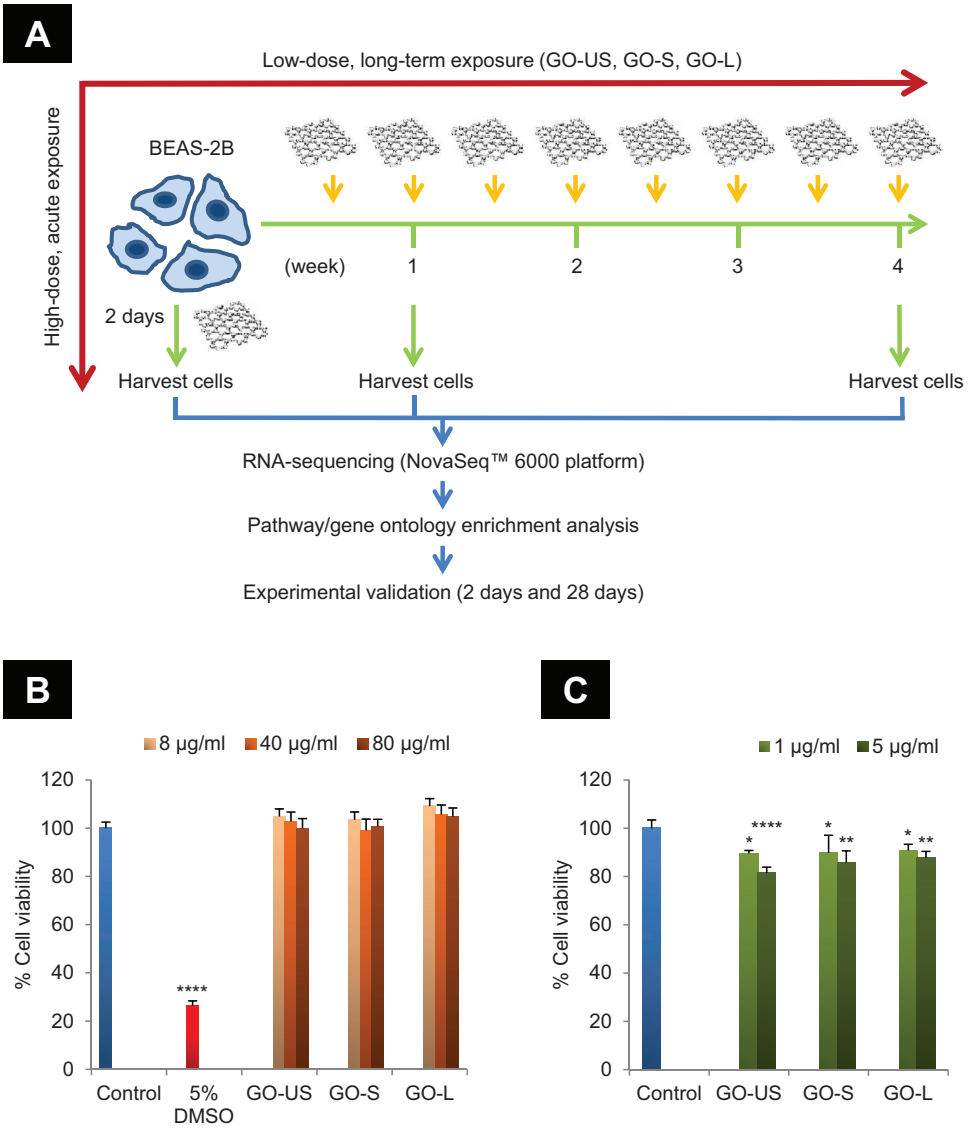


**Figure 1.** Long-term and short-term exposure to GO of varying lateral dimensions. A) Experimental design. The nontransformed human lung cell line BEAS-2B was exposed to GO-US, GO-S, and GO-L twice weekly for 4 weeks at 1 and 5 µg mL$^{-1}$, or to the cumulative dose (8 and 40 µg mL$^{-1}$) for 48 h; in addition, cells were exposed to 80 µg mL$^{-1}$ for 48 h. B) Cell viability assessment was performed with the Alamar blue assay after 48 h of exposure. DMSO was included as a positive control (****$p < 0.0001$). No significant differences were noted between the GO-exposed samples and the negative control (untreated cells). C) Cell viability assessment at 28 days of exposure. To this end, at 28 days, attached cells were harvested and replated for 24 h in fresh cell culture medium prior to cell viability (recovery) assessment. Statistical analysis conducted by one-way ANOVA with Dunnett's post hoc test. ****$p < 0.0001$, **$p < 0.01$, *$p < 0.05$.

Figure S2 (Supporting Information) shows the hierarchical cluster analysis of the top canonical pathways identified in BEAS-2B cells exposed to GO-US, GO-S, and GO-L for 2 days at 40 µg mL$^{-1}$. The color coding in the heatmap depicts the activation $z$-score for the pathways shown. Only DEGs with ≥0.5 log fold change and ≥0.05 FDR were included in the analysis. The results clearly showed size (i.e., lateral dimension) dependent changes. Similarly, the corresponding analysis was performed for BEAS-2B cells exposed to GO-US, GO-S, and GO-L for 2 days at 80 µg mL$^{-1}$, and the results, again, showed size-dependent differences in gene expression (Figure S3, Supporting Information). We then contrasted the results of the pathway analysis for samples obtained at 48 h versus 28 days (discussed below) at the corresponding, cumulative concentrations of GO-L (**Figure 3**). The results showed distinct differences at the pathway level between short-term and long-term exposures to GO-L, in line with the analysis conducted at the level of DEGs, as reported in Figure 2.

### 2.3. Validation of the Acute Impact of GO on Mitochondrial Dysfunction

We then leveraged the IPA software tool to examine the RNA-sequencing data with respect to toxicity pathways. This analysis identified the most affected toxicity endpoints following GO

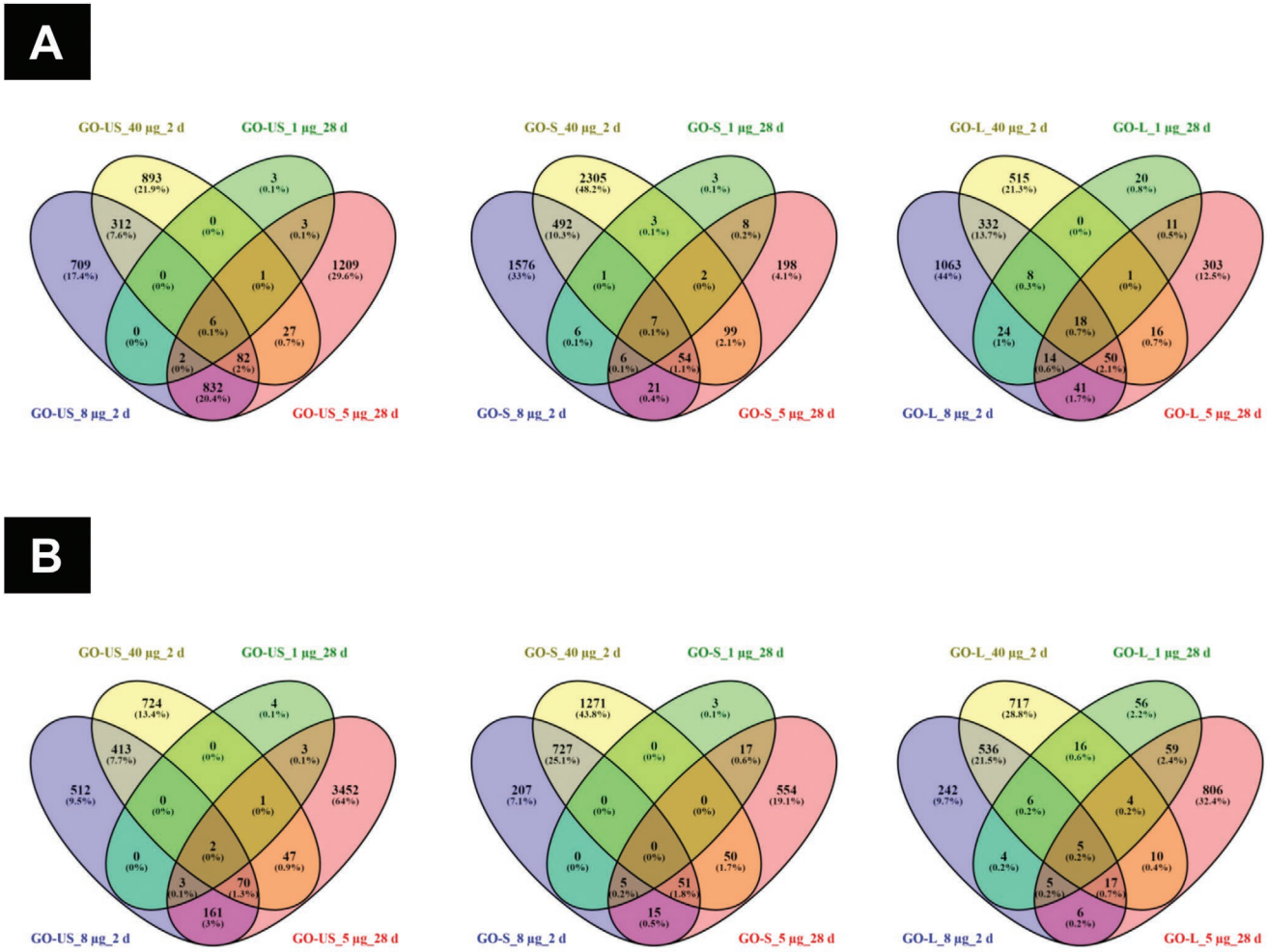


**Figure 2.** Venn diagrams of differentially expressed genes as determined by RNA sequencing of BEAS-2B cells exposed to GO-US, GO-S, and GO-L for 2 days (48 h) and 28 days. A) Comparison of upregulated genes exposed to GO-US, GO-S, and GO-L at the long-term 28 day repeated low dose exposure, i.e., 1 and 5 µg mL$^{-1}$, and at the 2 day cumulative high dose exposure, i.e., 8 and 40 µg mL$^{-1}$. B) Comparison of downregulated genes exposed to GO-US, GO-S, and GO-L at the same doses as in (A). DEGs having ≥0.5 log fold change and ≥0.05 FDR were included in the analysis.

exposure and may thus aid in deducing the mechanisms of toxicity. **Figure 4**a depicts the results of the latter analysis with respect to BEAS-2B cells exposed for 48 h to GO-US, GO-S, and GO-L at 40 µg mL$^{-1}$. The most significantly affected pathway for all three GO materials was "mitochondrial dysfunction". To validate these predictions, we exposed cells to GO-US, GO-S, and GO-L for 48 h and determined intracellular ATP levels (Figure 4b) as well as the mitochondrial membrane potential based on TMRE labeling (Figure 4c). We used FCCP, a potent uncoupler of mitochondrial oxidative phosphorylation, as a positive control. The results revealed a decrease in cellular ATP content (significant change observed for GO-L) and a concomitant increase in the dissipation of the mitochondrial membrane potential (significant changes noted for all three GO materials), in line with the RNA-sequencing data. To further examine the effects of GO on mitochondrial dysfunction, we studied the individual genes that were affected according to the RNA-sequencing analysis. Focusing on GO-L, we found that the "mitochondrial dysfunction" pathway was affected both at 40 and at 80 µg mL$^{-1}$, and less at 8 µg mL$^{-1}$ (**Figure 5**a). Moreover, genes encoding for different subunits of the mitochondrial ATP synthase as well as genes encoding different subunits of the cytochrome c oxidase were downregulated (Figure 5b).

Furthermore, as the pathway "hepatic fibrosis" was also affected by exposure to GO (Figure 4a), we looked more closely at the genes involved in this pathway and found that several genes encoding collagen proteins as well as pro-fibrotic factors such as members of the insulin-like growth factor binding protein family of proteins were affected (Figure S4a, Supporting Information). To evaluate this further, we determined total collagen secretion and deposition on cell culture plates after exposure for 48 h to GO-US, GO-S, and GO-L (plates were precoated with fibronectin and bovine serum albumin, but collagen was excluded). The amount of soluble collagen in the cell medium was not significantly affected (Figure S4b, Supporting Information). On the other hand, the acid soluble collagen, i.e., newly formed and deposited collagen, was increased in exposed cells (except in the case of GO-S administered at 80 µg mL$^{-1}$), and the total amount of collagen was increased

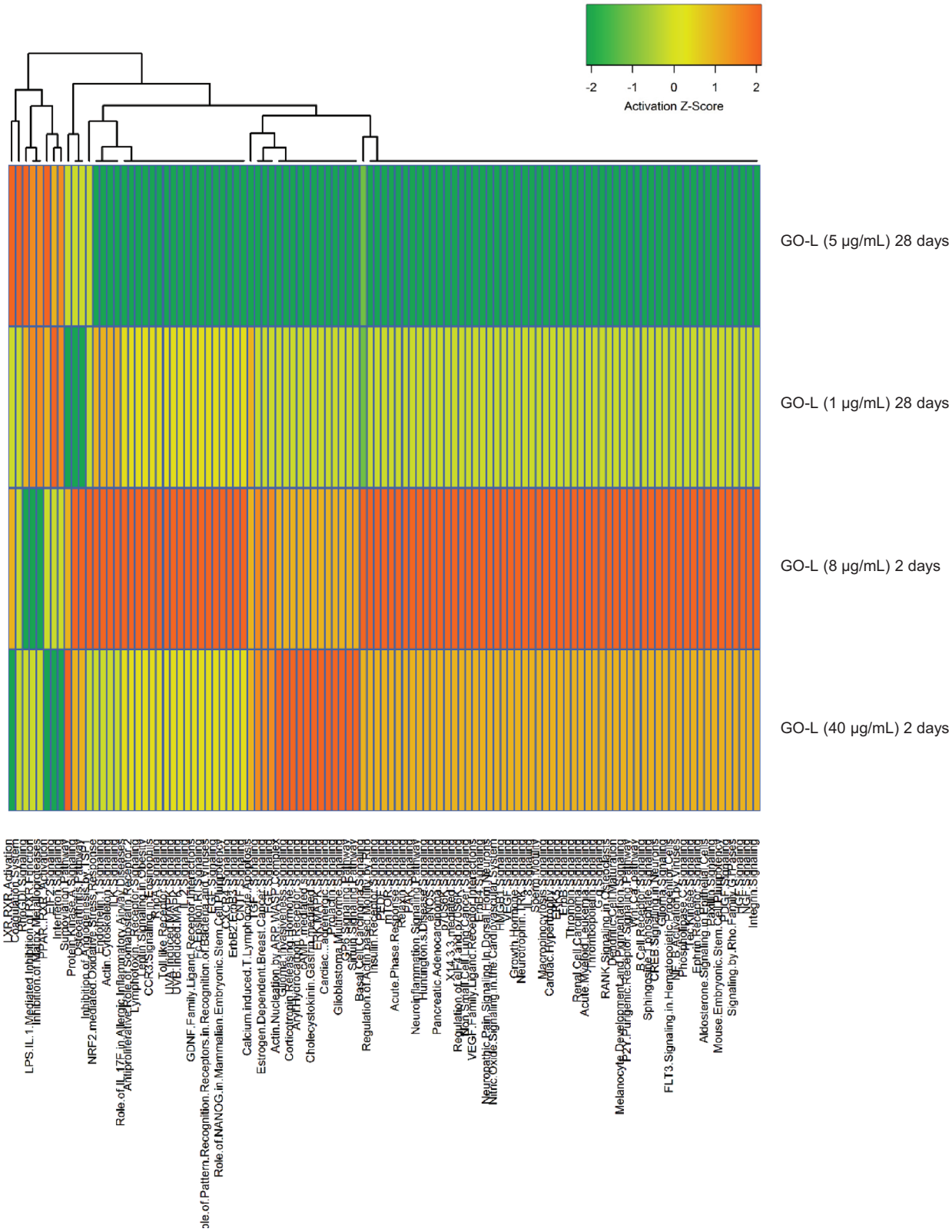


**Figure 3.** Downstream analysis of RNA-sequencing data reveals differences between acute and chronic exposure to GO. Hierarchical clustering analysis of the top canonical pathways identified by IPA in cells exposed to GO-L twice weekly for 4 weeks (28 days) at 1 and 5 µg mL$^{-1}$ versus cells exposed acutely (48 h) to the same cumulative doses, i.e., 8 and 40 µg mL$^{-1}$. DEGs having ≥0.5 log fold change and ≥0.05 FDR were included in the analysis. The color coding in the heatmap depicts the activation *z*-score for the pathways.

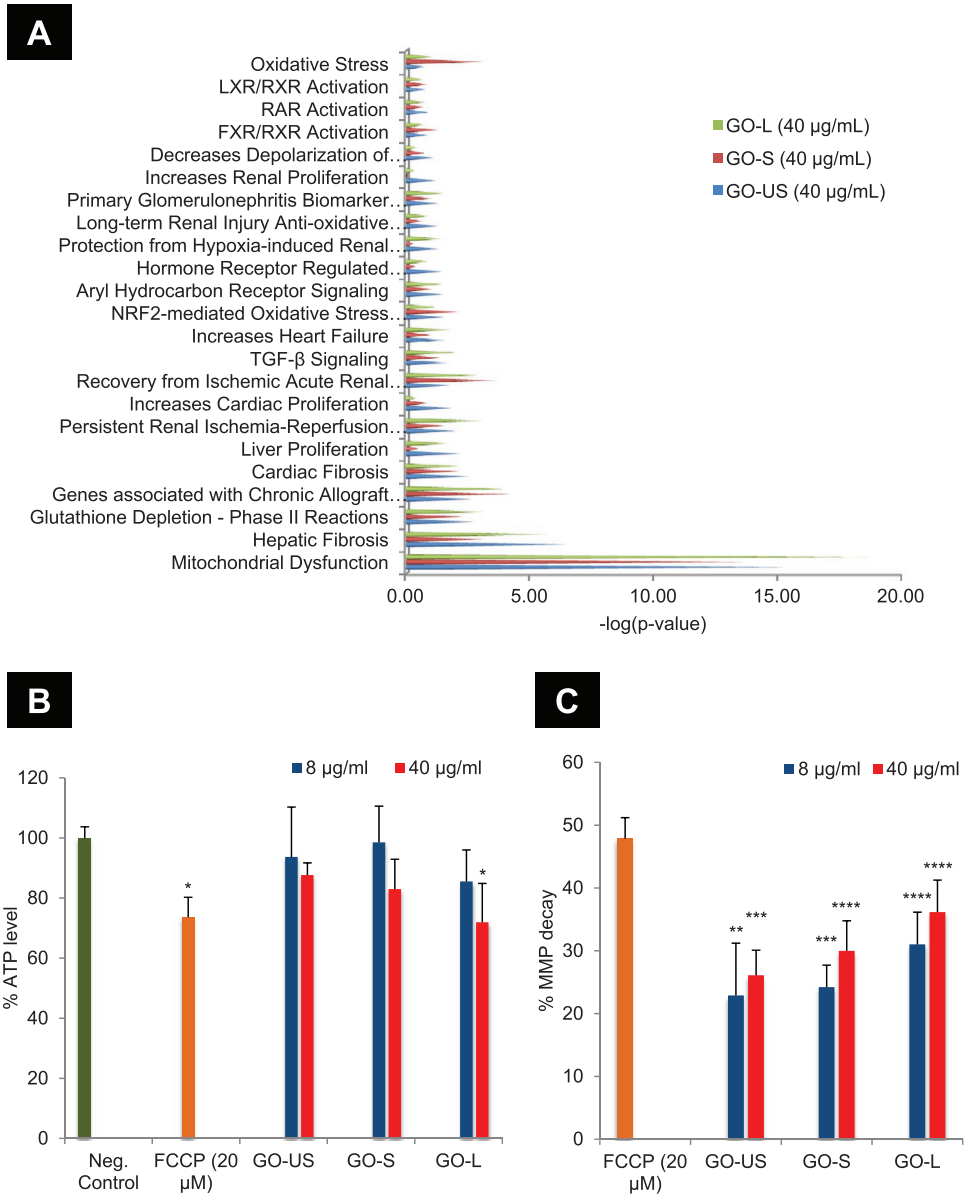


**Figure 4.** IPA analysis of RNA-sequencing data reveals mitochondrial dysfunction in exposed cells. A) The topmost affected toxicity pathways following exposure to GO-US, GO-S, and GO-L at 40 µg mL$^{-1}$ for 48 h. The pathways are ordered with respect to *p*-values. B) The validation study showed a decrease in intracellular ATP after exposure for 2 days to the indicated concentrations of GO. The mitochondrial uncoupling agent, FCCP, was used a positive control (*$p < 0.05$). C) Mitochondrial membrane potential decay was evidenced after exposure for 2 days to the indicated concentrations of GO. FCCP was used a positive control. Statistical analysis performed by one-way ANOVA with Dunnett's post hoc test. ****$p < 0.0001$, ***$p < 0.001$, **$p < 0.01$.

(albeit not for every treatment) (Figure 4Sb, Supporting Information). The results showed, overall, that GO has the potential to interfere with collagen secretion and deposition if administered at a high dose.

### 2.4. Transcriptional Responses Following Long-Term Exposure to GO

Next, we subjected BEAS-2B cells to long-term, low-dose exposure of GO. BEAS-2B cells were thus exposed to GO-US, GO-S, and GO-L for 28 days at 1 and 5 µg mL$^{-1}$. We noted a modest decrease in cell viability by using the Alamar blue assay (Figure 1c). For the latter assay, cells exposed to GO for 4 weeks were reseeded and maintained for 24 h in fresh medium without GO prior to analysis; hence, the results are reflective of cell *recovery* following long-term exposure to GO. Next, BEAS-2B cells exposed to GO at the indicated concentrations were harvested at day 7 and at day 28 for RNA sequencing using the Illumina NovaSeq 6000 sequencing platform, as described above for the short-term samples. The number of DEGs affected by GO was, overall, lower at day

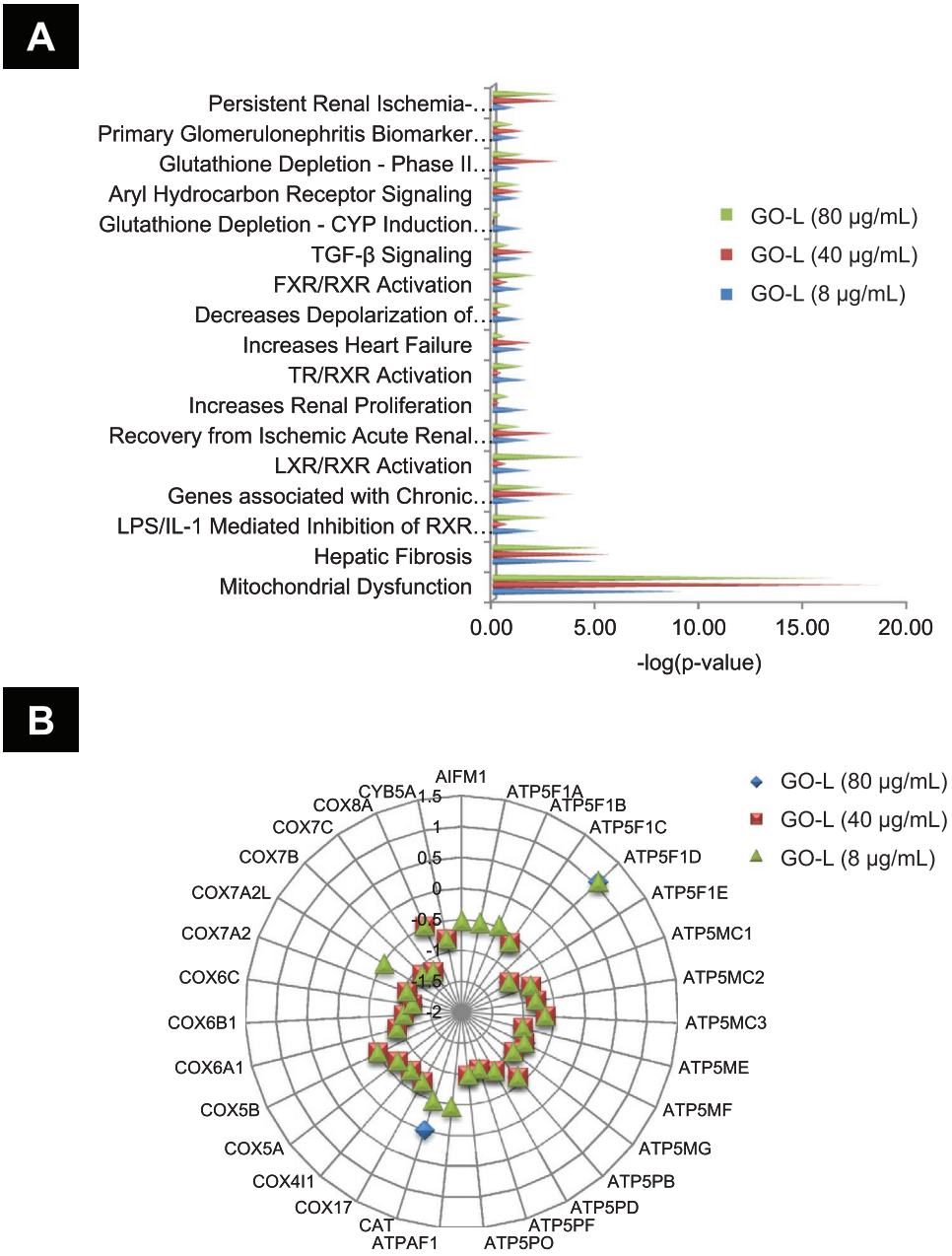


**Figure 5.** IPA analysis of RNA-sequencing data reveals mitochondrial dysfunction in exposed cells. A) The topmost affected toxicity pathways following exposure of BEAS-2B cells for 48 h to GO-L at 8, 40, and 80 µg mL$^{-1}$. The pathways are ordered with respect to *p*-values. B) The genes involved in the "mitochondrial dysfunction" pathway for GO-L at 8, 40, and 80 µg mL$^{-1}$. The *Y* axis represents the expression log ratio.

28 as compared to the 48 h samples (Table S2, Supporting Information). Notably, cells exposed to GO-US (5 µg mL$^{-1}$) displayed the highest number of DEGs with more down- than upregulated genes. Additionally, cells exposed to 5 µg mL$^{-1}$ of GO-US displayed a greater number of affected genes when compared to GO-S and GO-L, as evidenced in the volcano plots (Figure S5, Supporting Information) and in the Venn diagrams (Figure 2). Furthermore, the number of DEGs at day 28 exceeded those at day 7 (Figure S6, Supporting Information). For the subsequent bioinformatics analyses, we therefore focused on the 28 day samples.

#### *2.4.1. Canonical Pathway Enrichment Analysis*

We used IPA to interpret the RNA-sequencing data by performing canonical pathway enrichment analysis. **Figure 6** shows the hierarchical cluster analysis of the top canonical pathways identified in BEAS-2B cells exposed to GO-US, GO-S, and GO-L for 28 days at repeated doses of 1 and 5 µg mL$^{-1}$. Only DEGs with ≥0.5 log fold change and ≥0.05 FDR were included in the analysis. Overall, long-term, low-dose exposure to GO was found to trigger downregulation of pathways, as shown by the negative activation scores (Figure 6).

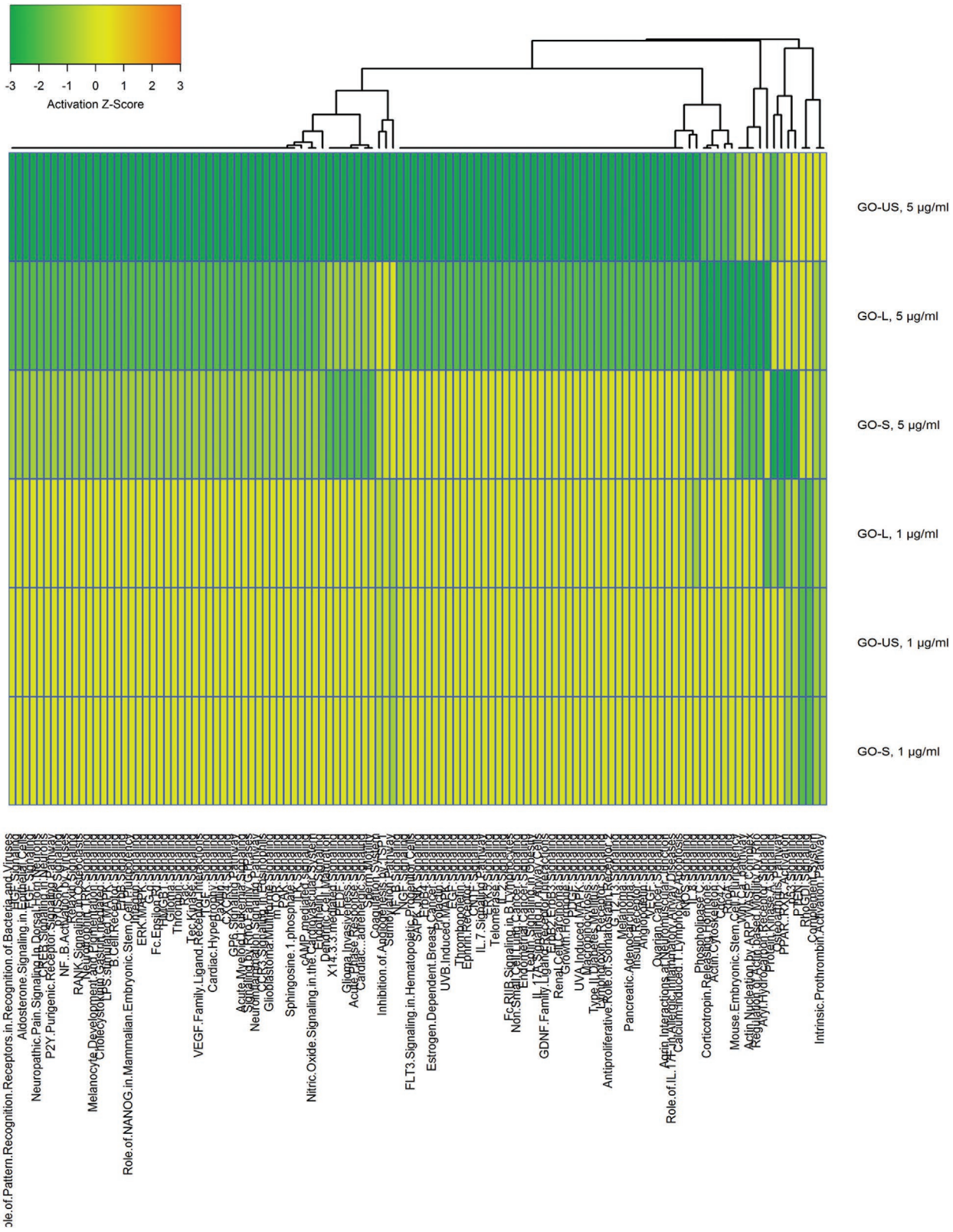


**Figure 6.** Downstream analysis of RNA-sequencing data following low-dose, repeated exposure to GO of varying lateral dimensions. Hierarchical clustering analysis of the top canonical pathways identified in BEAS-2B cells exposed to GO-US, GO-S, and GO-L twice weekly for 28 days at 1 and 5 μg $mL^{-1}$. DEGs having ≥0.5 log fold change and ≥0.05 FDR were included in the analysis. The color coding depicts the activation *z*-score for the pathways. Hence, all pathways were found to be downregulated, with the most pronounced effects noted for ultrasmall GO at 5 μg $mL^{-1}$.

*2.4.2. Toxicity Pathway Enrichment Analysis*

We used IPA to shed light on the putative mechanism(s) of toxicity triggered by long-term exposure to GO. As shown in Figure S7 (Supporting Information), several pathways related to cell proliferation and/or cell death were affected by all three GO materials, as evidenced by their *p*-values (results shown for the 5 μg $mL^{-1}$ samples). Looking more closely at the pathway designated as "liver necrosis/cell death" in the IPA knowledge base, we noted several genes implicated in the regulation of apoptosis, both for GO-US (Figure S8, Supporting Information), GO-S (Figure S9, Supporting Information), and GO-L (Figure S10, Supporting Information). We therefore queried the RNA-sequencing data specifically with regards to apoptosis genes. Focusing on the transcriptomics results obtained in cells exposed for 28 days to GO-US (5 μg $mL^{-1}$), we found that several pro-apoptotic genes belonging to the Bcl-2 family[25] including *BAX*, *BAK*, and *BAD* were upregulated, while several antiapoptotic genes belonging to the inhibitor of apoptosis protein (IAP) family[26] such as *BIRC6* encoding a very large (528 kDa) protein known as Apollon were downregulated (RNA-seq data shown in schematic form in **Figure 7**a, with expression levels in Figure 7b).

### 2.5. Validation of the Long-Term Impact of GO on Apoptosis Induction

To validate the transcriptomics results depicted in Figure 7a, we focused on *BIRC2* (cIAP-1) and *BIRC6* (Apollon), key regulators of caspase activation downstream of mitochondria.[26] To this end, BEAS-2B cells were subjected to long-term, low-dose exposure to GO-US, GO-S, and GO-L for 28 days at repeated doses of 1 and 5 μg $mL^{-1}$. Then, cell samples were harvested and examined with respect to the expression of Apollon and cIAP-1. As shown in Figure 7c, GO exposure resulted in a decreased expression of both proteins, thus confirming the RNA-sequencing results. GAPDH was probed to control for equal loading of the samples. Caspase activation leads to cleavage of a number of cellular target proteins including the nuclear protein, poly(ADP-ribose) polymerase (PARP).[27] We therefore evaluated PARP cleavage in BEAS-2B cells exposed for 28 days to GO. As shown in Figure 7d, exposure to GO-US, in particular, but also exposure to GO-S and GO-L, resulted in the cleavage and loss of full-length PARP yielding a cleavage fragment indicative of caspase activation. To further assess whether long-term exposure to GO is capable of triggering apoptosis in lung cells, we determined apoptosis by using the classical DNA content assay whereby apoptotic cells are identified on the basis of a reduction of their DNA content.[28] To this end, BEAS-2B cells were exposed to GO at repeated doses of 1 and 5 μg $mL^{-1}$ for 1, 2, 3, or 4 weeks and cells were then harvested for flow cytometric analysis. Untreated cells showed no increase in apoptosis during the course of the experiment (**Figure 8**). In contrast, dose- and time-dependent apoptosis was observed in response to GO-US, GO-S, and GO-L, in line with the RNA-sequencing data.

## 3. Discussion

Using RNA sequencing, we showed herein that human lung cells respond differently to acute versus long-term exposure to GO. Our study thus demonstrated the utility of RNA-sequencing approaches in terms of dissecting low-dose cellular responses to GO. Previous studies of CNTs[16,29] and silver nanoparticles[30] using the same cell model have shown malignant transformation of lung cells upon long-term exposure (i.e., weeks to month). However, in the present study we found no signs of oncogenic transformation of BEAS-2B cells. Instead, short-term exposure resulted in mitochondrial dysfunction (in the absence of cell death) while long-term exposure affected the apoptosis sensitivity of the cells. Previous studies have disclosed pronounced effects of GO on mitochondria in the human immortalized keratinocyte cell line, HaCaT, a commonly used model of skin cells.[31,32] Others have reported that GO triggered cell death with a concomitant drop of the mitochondrial membrane potential in the hepatocellular carcinoma cell line, HepG2.[33] On the basis of pathway analysis of microarray results, the authors concluded that TGF$\beta$1-mediated signaling played a central role in GO-induced cellular effects. Pristine graphene was also shown in a previous study to engage TGF$\beta$1-dependent signaling pathways in a murine macrophage cell line, leading to cell death.[34] This is noteworthy as our analysis of upstream regulators of GO-induced transcriptional responses also implicated TGF$\beta$1 as one of the regulators in the BEAS-2B model (unpublished observations). The previous studies cited here were all short-term studies using relatively high doses of GBMs. In contrast, few low-dose studies of GBMs have been published to date. Using zebrafish embryos as a model, Zhang et al.[35] reported on the developmental toxicity of GO (single-layer GO, ≈0.3 to 2.6 μm in lateral size) at predicted environmental concentrations (1-100 μg $L^{-1}$). The authors conducted gene expression analyses of embryos exposed to 100 μg $L^{-1}$ of GO from 2.5 hpf to 7 dpf by using RNA sequencing. Notably, gene ontology enrichment analysis revealed downregulation of genes related to the extracellular matrix, including several collagen-encoding genes; additionally, two matrix metalloproteinase (MMP) genes (*mmp9* and *mmp13a*) were shown to be upregulated by GO. In the present study, we noted the upregulation of several collagen-encoding genes as well as *MMP9* following exposure of human lung cells to GO. We noted a corresponding increase in collagen production in BEAS-2B cells exposed for 48 h to GO. However, we did not observe any significant upregulation of collagen-encoding genes at 28 days of exposure, even though *MMP9* was affected. The role of MMP upregulation in response to GO exposure in lung cells thus remains to be clarified. Furthermore, we recently concluded a long-term (90 day) follow-up of mice acutely exposed to the same GO via the pulmonary route and we did not observe any lung fibrosis.[36] The deregulation of collagen production in GO-exposed lung cells may be a transient cellular response to stress.

Choosing relevant in vitro models is important for the proper evaluation of nanomaterials. The A549 adenocarcinoma cell line is commonly used as a model of the lung epithelium; however, it is important to consider that these cells are malignant, and therefore cannot be expected to respond like normal cells.

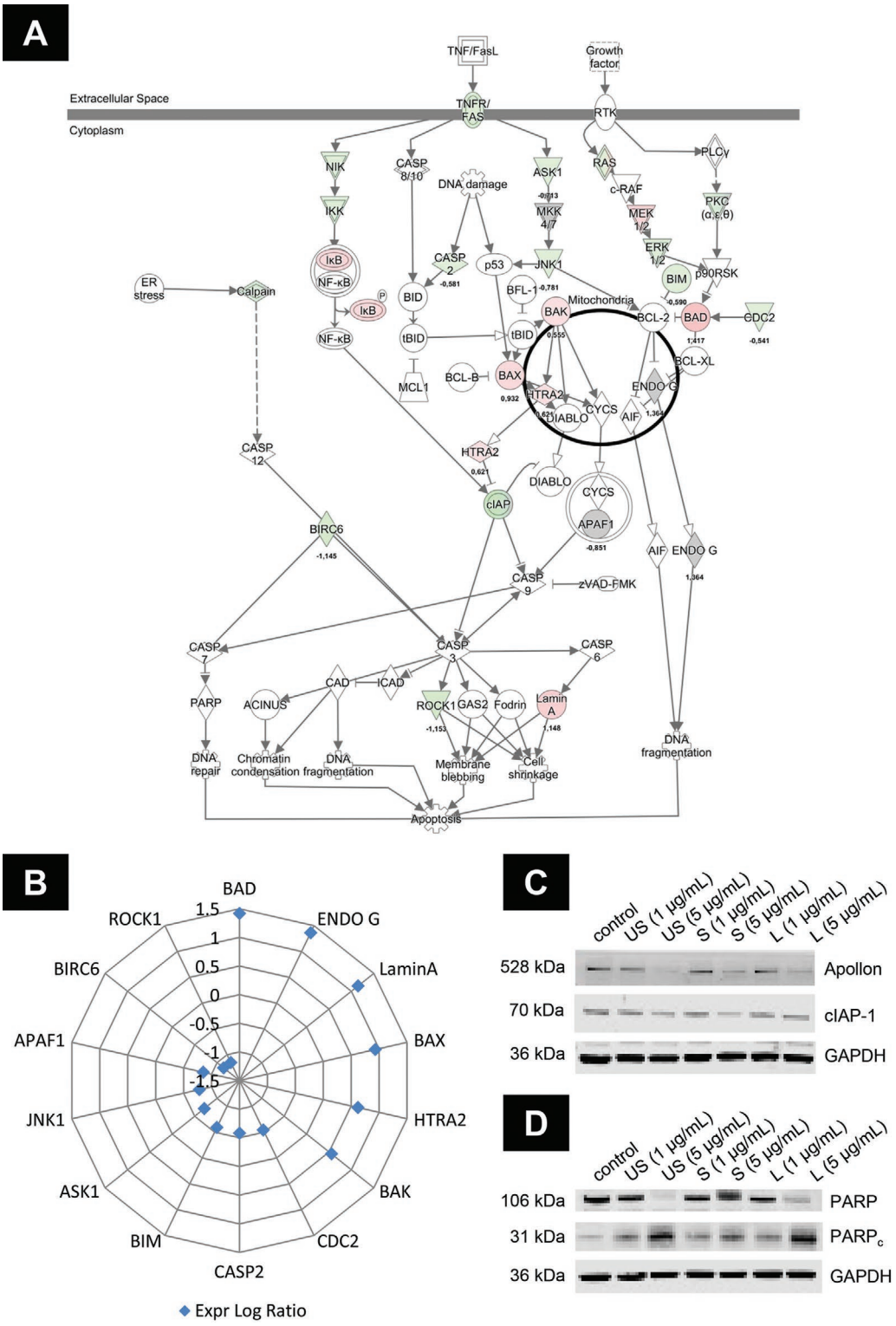


**Figure 7.** Long-term exposure to GO leads to the deregulation of apoptosis signaling pathways. A) IPA analysis of RNA-sequencing data of BEAS-2B cells exposed to GO-US (5 μg mL$^{-1}$) for 28 days revealed significant perturbations of the mitochondria-dependent apoptosis pathway, with upregulation (red) of pro-apoptotic genes, and downregulation (green) of antiapoptotic genes, including *BIRC6* (encoding Apollon/Bruce). B) The expression level of the genes involved in the apoptosis pathway depicted in (A). The *Y* axis represents the expression log ratio. C) The validation study confirmed that the expression of Apollon and cIAP-1 was lost or reduced in cells exposed to GO-US, GO-S, and GO-L for 28 days at 1 and 5 μg mL$^{-1}$. GAPDH was included as a loading control. D) PARP cleavage indicative of caspase activation as evidenced by Western blot (i.e., reduction of full-length PARP and a concomitant increase in cleaved PARP). GAPDH was included as a loading control.

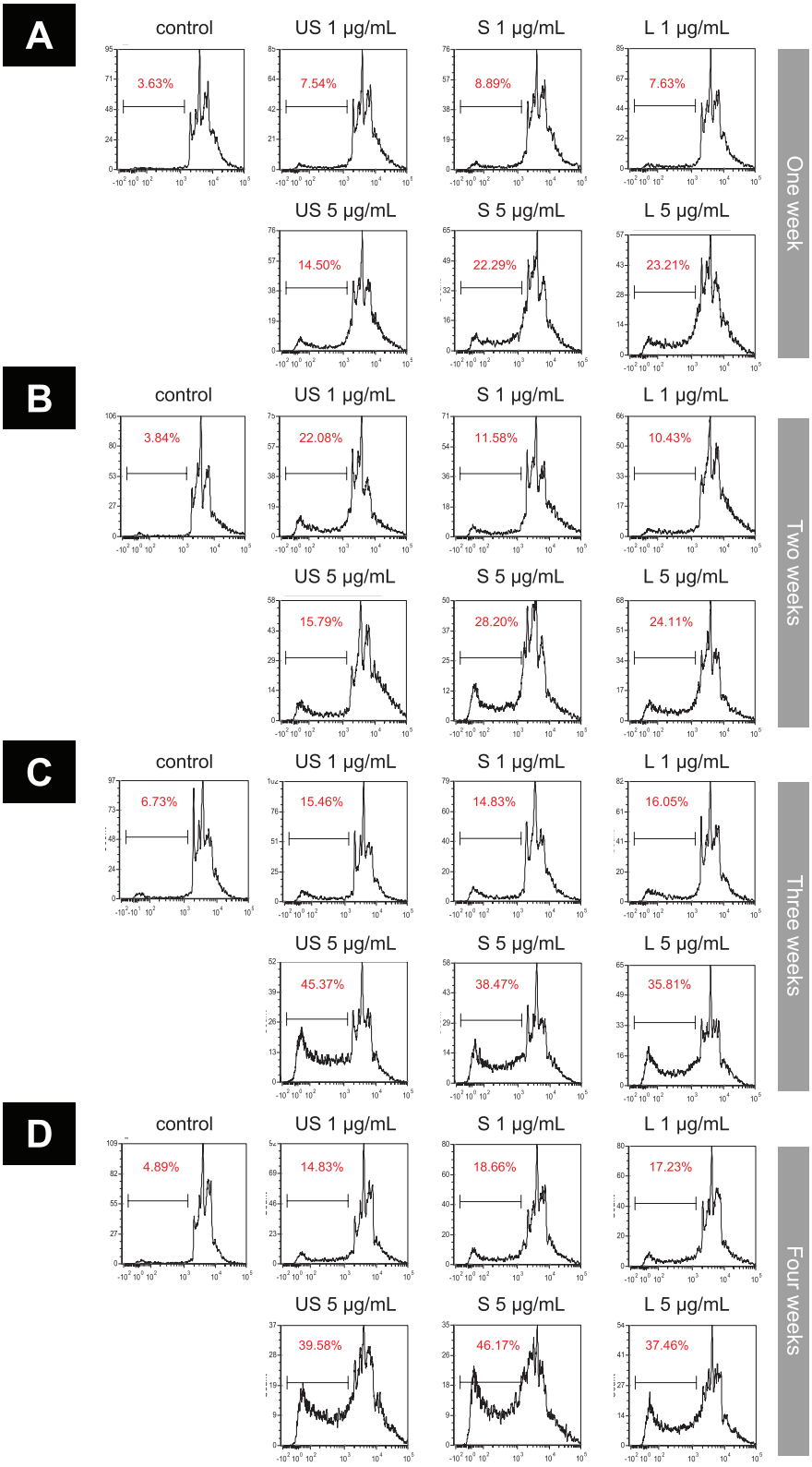


**Figure 8.** Long-term exposure to GO affects the susceptibility of lung cells to apoptosis. To validate the RNA-sequencing-based prediction regarding apoptosis, we exposed BEAS-2B cells to GO-US, GO-S, and GO-L twice weekly for 28 days at 1 and 5 μg $mL^{-1}$, and harvested cells at weekly intervals A–D) for analysis using the DNA content assay. Untreated control cells maintained in culture under the same conditions were included for comparison. The results showed a dose- and time-dependent increase of apoptosis following low-dose exposure to GO while control cells were unaffected.

Moreover, the cells are typically cultured in the cell medium containing 10% fetal bovine serum, which is not a natural biological medium for lung cells. In a previous study, we compared the A549 cell line with primary human bronchial epithelial cells (PBECs) and could show that palladium nanoparticles triggered caspase-dependent apoptosis in PBECs, but not in the A549 cell line.[37] Furthermore, we could show, in a subsequent study using cationic dendrimers, that the A549 cell line was markedly less sensitive to cell death when compared to PBECs.[4] In the present study, we opted for the human, immortalized (nontumorigenic) BEAS-2B cell line as a suitable model of the bronchial epithelium. We and others have previously shown that these cells are suitable for long-term studies of nanomaterials including single-walled CNTs and silver nanoparticles.[16,18,30] The advantage of using a human cell line as a model is that the interindividual variation is reduced. It is also important to point out that functional validation of transcriptomics data is needed to anchor the omics results in a biologically meaningful context; in the absence of validation, omics-based approaches serve mainly to catalog changes in gene and protein expression.[38] Granted, such studies are also useful as a means of profiling and contrasting different (nano)materials, though they fall short of describing the underlying mechanism of toxicity. In the present study, functional validation, performed on an independent set of samples, clearly demonstrated that RNA sequencing can be harnessed to dissect cellular responses to GO with varying lateral dimensions, and we could show that acute and long-term exposures trigger distinct outcomes.

Understanding nanomaterial-induced perturbations of different cell death programs may allow for a better prediction of the health hazards of these materials.[39] In the present study, we could show that GO of varying lateral dimensions, from the submicron range up to several tens of micrometers, are capable of reprogramming lung cells such that the apoptosis threshold is affected, leading to a greater susceptibility to caspase-mediated apoptosis. In particular, we noted that exposure to GO caused a marked downregulation of different IAP family members, including cIAP-1, encoded by *BIRC2*, and Apollon (known as Bruce in mice), encoded by *BIRC6*. Importantly, XIAP, cIAP-1, and cIAP-2 are capable of directly inhibiting certain caspases including caspase-3.[26] This differs from the effects of the Bcl-2-related proteins, which function upstream in the cell death pathway, at the level of mitochondria, to regulate caspase-mediated apoptosis.[40] Apollon is an exceptionally large BIR (baculoviral IAP repeat) domain-containing protein that has been implicated as a key regulator of apoptosis and cell division.[41,42] Moreover, recent work has suggested that Apollon also regulates autophagosome-lysosome fusion.[43] Apollon binds to, ubiquitinates, and promotes proteasomal degradation of second mitochondrial activator of apoptosis (Smac) and caspase-9, thus preventing mitochondria-dependent apoptosis.[44] Apollon is unique due to its size and because it is bound to membranes of the trans-Golgi network and other vesicular structures.[43] As a result, it has been suggested that Apollon may not act as a general caspase inhibitor, but as a specialized regulator of caspase activity at cellular membranes. Notably, decreasing the expression of Apollon/Bruce is sufficient to trigger apoptosis.[41] The present study is the first to show that low-dose exposure to a nanomaterial can elicit the transcriptional downregulation of *BIRC6* and, consequently, the loss of Apollon expression. We confirmed the occurrence of caspase-mediated apoptosis by the detection of PARP cleavage, and by using the classical DNA content assay. Overall, we have conclusively shown that long-term exposure to GO sheets of varying lateral dimensions affects the apoptosis threshold in human bronchial epithelial cells.

The question arises as to the possible in vivo relevance of this increased apoptosis susceptibility? The lung epithelium presents both a physical and immunological barrier between our body and the external environment. Interestingly, compensatory cell proliferation in response to apoptosis of epithelial cells has been documented.[45] Furthermore, epithelial cell apoptosis in the lungs and in the gut was found to play a role in maintaining regulatory T cell numbers.[46] Hence, apoptosis induction and the weeding out of dying cells exposed to GO could promote tissue integrity and function.[47] However, this is presently a matter of conjecture and further studies are needed.

## 4. Conclusions

In summary, we have shown that RNA sequencing can be used to probe cellular responses to GO even at relatively low doses. Specifically, we have demonstrated distinct differences in the pattern of differentially expressed genes in human lung cells subjected to low-dose, long-term exposure versus high-dose, short-term exposure to GO sheets of varying lateral dimensions. Detailed bioinformatics analyses of the transcriptomics data coupled with functional validation showed that acute exposure resulted in mitochondrial dysfunction (cellular stress) in the absence of overt cell death while chronic or repeated exposure to GO resulted in a gradual sensitization to apoptosis induction accompanied by upregulation of pro-apoptotic genes belonging to the Bcl-2 family and downregulation of antiapoptotic genes belonging to the IAP family. Overall, the present findings suggest that conventional, short-term assays are insufficient if we are to capture the biological responses of GO; long-term studies of GO are also required. In general, the research community should rethink nanosafety in terms of assays and model systems to make sure that they are as realistic as possible.

## 5. Experimental Section

*GO Synthesis and Characterization*: GO sheets of three different sizes, i.e., ultrasmall (GO-US), small (GO-S), and large (GO-L), were produced from graphite flakes using a modified Hummers' method.[14] Detailed physicochemical characterization of the GO sheets has been reported,[14] and a summary of the results is provided in Table S1 (Supporting Information).

*Endotoxin Content*: GO samples were evaluated for potential endotoxin content by using the TNF-$\alpha$ expression test (TET) as previously described.[48] In brief, human monocyte-derived macrophages (HMDMs) were generated from buffy coats obtained from healthy human blood donors (Karolinska University Hospital, Stockholm, Sweden). Cell viability was evaluated by using the Alamar blue assay and a noncytotoxic dose of GO was selected for subsequent assessment of TNF-$\alpha$ production. HMDMs were thus exposed to GO (50 µg mL$^{-1}$) or LPS (Sigma-Aldrich) in the presence or absence of the specific LPS inhibitor, polymyxin B ($10 \times 10^{-6}$ M) (Sigma-Aldrich) and TNF-$\alpha$ secretion was measured by using the Human TNF-$\alpha$ ELISA from Abcam (Sweden).

*BEAS-2B Cell Culture*: The immortalized human bronchial epithelial cell line, BEAS 2B (European Collection of Cell Cultures) was maintained in bronchial epithelial cell growth medium (BEGM, Lonza) supplemented with BEGM bullet-kit (Lonza) (recombinant epidermal growth factor (EGF), bovine pituitary extract, GA-1000 (gentamicin sulfate and amphotericin-B), hydrocortisone, insulin, retinoic acid, transferrin, triiodothyronine, and epinephrine). Cells were cultured in flasks and plates precoated with 0.01 mg $mL^{-1}$ fibronectin, 0.03 mg $mL^{-1}$ bovine collagen type I, and 0.01 mg $mL^{-1}$ bovine serum albumin in BEGM additive free medium for 2 h prior to the seeding. Cells were maintained in a humidified atmosphere at 37 °C, 5% $CO_2$ and subcultured at 80% confluency. For short-term exposure (48 h), BEAS-2B were seeded in 6 well-plates ($2.5 \times 10^4$ cells $mL^{-1}$) and were allowed to attach for 3 h prior to the exposure. For long-term exposure (up to 28 days), BEAS-2B were seeded in T25 flasks ($2.5 \times 10^4$ cells $mL^{-1}$) and allowed to attach for 3 h prior to the exposure. After cell attachment, cells were exposed to GO. For long-term experiments, cells were exposed for 7 and 28 days, in triplicate, to 1 and 5 µg $mL^{-1}$ GO. To this end, the cells were split, counted, reseeded twice a week ($2.5 \times 10^4$ cells $mL^{-1}$) and re-exposed to the respective GOs. While for short term exposure, cells were exposed for 48 h to 8, 40, or 80 µg $mL^{-1}$. The long-term experiment was performed twice: the initial experiment was performed for RNA sequencing, while the experiment was repeated a second time for the other assays for the purpose of validating the transcriptomics results (Figure 1a).

*Alamar Blue Assay*: Cell viability was evaluated following GO exposure by using the Alamar blue assay (ThermoFischer Scientific). Alamar blue (resazurin) is a nonfluorescent, cell permeable compound. Upon entering cells, resazurin is reduced to resorufin in viable cells, which produces a red fluorescence. For the low-dose, long-term exposure, cells were harvested, counted, and reseeded in 96-well plates ($10^5$ cells $mL^{-1}$). Cells were maintained in standard growth medium (BEGM) without GO for 24 h. The medium was then removed and replaced with 10% Alamar blue solution (ThermoFischer Scientific) prepared in cell culture medium and allowed to incubate for 3 h at 37 °C. Fluorescence (Ex560/Em590) was recorded using a plate reader (Tecan Infinite F200) operating with Magellan software. Background fluorescence was extracted from the total fluorescence of each well. Cell viability was calculated as % viability wherein the control was set at 100% and data are presented as mean values ± S.D. For the short-term exposure, cell medium was removed at 48 h and replaced with 10% Alamar blue solution prepared in cell culture medium, as above. Cells were allowed to incubate for 3 h at 37 °C and the samples were evaluated as described above.

*Mitochondrial Potential*: The mitochondrial membrane potential in cells exposed for 48 h to GO was determined by using the TMRE-Mitochondrial Membrane Potential Assay Kit (abcam). TMRE (tetramethylrhodamine, ethyl ester) is a cell permeable dye that readily accumulates in active mitochondria due to their relative negative charge and thereby labels active mitochondria.[49] Depolarized or inactive mitochondria have decreased membrane potential and fail to sequester TMRE. FCCP (carbonyl cyanide 4-(trifluoromethoxy) phenylhydrazone), which is an uncoupler of oxidative phosphorylation was used as a positive control at $20 \times 10^{-6}$ M (cells were exposed for 10 min).

*ATP Assay*: Total cellular ATP content was quantified using a luminescence-based Cell Viability Kit SL (BioThema, Sweden), according to the manufacturer´s protocol. Luminescence was detected using an Infinite F200 Tecan plate reader (Männendorf, Switzerland).

*Cell Cycle/Apoptosis Assay*: Apoptosis was quantified by using propidium iodide (PI) staining of the cells exposed to GO at 1 and 5 µg $mL^{-1}$ for 1, 2, 3, and 4 weeks, respectively. Briefly, after exposure the cells were first washed with PBS, fixed in 70% ice cold ethanol, and stored at 4 °C for at least 24 h prior to flow cytometric analysis. After collecting the samples, the cells were incubated with RNAse A (1 mg $mL^{-1}$) and propidium iodide (40 µg $mL^{-1}$) for 48 h in the dark at 4 °C. DNA content was analyzed on a BD LSRFortessa cell analyzer operating with FCS Express 4 Flow software. The assay is based on the principle that apoptotic cells are characterized by DNA fragmentation and formation of apoptotic "bodies" with a consequent loss of DNA content.

*Collagen Assay*: Collagen secretion and deposition was evaluated using the Sircol assay kit (Biocolor) as previously described.[30] To this end, cell supernatants were collected as well as the collagen deposited in the wells and samples were concentrated 15 times by incubating with the isolation and concentration reagent at 4 °C overnight. The pellets were mixed with the Sircol dye reagent. A standard curve was prepared from the collagen reference in the kit. Soluble collagen secreted in the cell medium and acid extracted collagen (insoluble collagen deposited in the well) was expressed as µg $mL^{-1}$.

*Western Blot*: Protein expression was analyzed using standard protocols.[28] First, the cells were washed in PBS and lysed in RIPA lysis buffer supplemented with a protease inhibitor cocktail (SigmaAldrich). Total protein content was quantified using a BCA Protein Assay Kit (ThermoFischer Scientific). Cell samples (10 µg protein) were separated by electrophoresis using a NuPAGE 4–12% bis–tris protein gel (Invitrogen, Sweden) followed by transfer to a PVDF membrane (Amersham). The blots were blocked with Odyssey Blocking Buffer (LI-COR Biosciences). Then, the following primary antibodies were applied: anti-cIAP1 antibody (ab108361), and anti-BIRC6 antibody (ab19609), from abcam (Cambridge, UK), and anti-GAPDH purchased from Sigma Aldrich (Sweden). Membranes were washed and probed with IRDye 800CW goat antirabbit secondary antibody and detection was performed on an Odyssey CLx LI-COR Biosciences scanner.

*RNA Extraction*: Total RNA was extracted from cells harvested at 48 h, 7 days, and 28 days of exposure to GO-US, GO-S, and GO-L using the RNeasy Mini Columns (Qiagen) in accordance with manufacturer's instructions (including the purification step with DNase I). Total RNA concentration was determined spectrophotometrically using NanoDrop (NanoDrop Technologies). Quality control was conducted using the Bioanalyzer 2100 (Agilent Technologies) and all samples had RNA integrity numbers (RIN) above 8. Triplicates of each sample at different time-points and exposures were submitted for sequencing. The samples included 8, 40, and 80 µg $mL^{-1}$ of GO-US, GO-S and GO-L and negative control (at 48 h), and repeated exposures to 1 and 5 µg $mL^{-1}$ of GO-US, GO-S and GO-L (at 7 and 28 days) along with negative controls.

*Library Preparation and Sequencing*: Illumina TruSeq Stranded mRNA Library Prep Kit (Illumina, Inc., San Diego, CA) was used to prepare mRNA sequencing libraries. Briefly, 1000 ng of total RNA was used for mRNA isolation using poly dT-coated beads. After purification, the mRNA was chemically fragmented into small pieces, which was subsequently used as a template for cDNA synthesis using reverse transcriptase followed by short fragment removal from another purification step. After end repair, adapter ligation, and index code adding for each sample, PCR amplification was conducted. Unaligned adapters were removed twice after adapter ligation and PCR amplification. The quality of the libraries was examined by Caliper LabChip GX/HT DNA high sensitivity and the quantitation of libraries were measured by Qubit dsDNA HS. The libraries were paired-end sequenced on a NovaSeq 6000 sequencing system (Illumina, Inc.). The conversion to FastQ was performed using bcl2fastq2 v2.19 from the CASAVA software suite. The quality scale used was Sanger/phred33/Illumina 1.8+.

*Sequencing Data Analyses*: The quality check involving the analysis of sequence quality, GC content, the presence of adaptors, overrepresented sequences, duplication level in order to detect sequencing errors, PCR artifacts or adapter contaminations was conducted using FastQC. The mRNA sequencing data were analyzed using the rnaseq pipeline (https://github.com/nf-core/rnaseq), a bioinformatics analysis pipeline specifically adapted for RNA sequencing. The workflow processed the raw data from FastQ inputs starting with quality and adapter trimming as well as quality control using Trim Galore! (https://www.bioinformatics.babraham.ac.uk/projects/trim_galore/) and then the preprocessed sequencing reads were aligned against the human reference genome GRCh37 using STAR.[50] Subsequently, the read counts to genes were generated using featureCounts.[51] Full-length transcripts representing multiple splice variants for each gene locus were assembled and quantitated using StringTie.[52] Extensive quality control of the results was performed using RSeQC,[53] dupRadar,[54] and Preseq (http://smithlabresearch.org/software/preseq/) which generated

RNA quality control metrics, technical/biological read duplication level and library complexity estimation.

*Bioinformatics Analyses*: Differentially expressed genes (DEGs) between different treatments were determined using edgeR.[22] The table of integer read counts that as produced by featureCounts from the rnaseq pipeline was used as input. Trimmed mean of *M*-values (TMM) normalization was applied to the dataset to account for compositional difference between the libraries. Likelihood-ratio test was performed to determine DEGs. Differential gene expression levels between the negative control samples and the GOs (i.e., GO-US, GO-S, and GO-L) were estimated with a *t*-test and the *p*-values were corrected with the Benjamini–Hochberg algorithm (false discovery rate, FDR). DEGs having a fold change (log FC) ≥ 0.5 and *p*-values ≤ 0.05 were considered for functional analysis. After finalizing the list of DEGs, enriched networks, molecular functions, and pathways were generated using the ingenuity pathway analysis (IPA) software (QIAGEN Inc., Redwood City, CA). IPA was also used to explore upstream regulators, as previously described.[55] Volcano plots were generated by plotting derived by plotting $-\log_{10}$(FDR adjusted *p*-value) in relation to the $\log_2$(fold change) using the EnhancedVolcano (https://github.com/kevinblighe) and ggplot2 and ggrepel packages in R. Venn diagrams were plotted with a web-based tool developed by the Bioinformatics and Evolutionary Genomics Laboratory at VIB/UGent, Belgium (http://bioinformatics.psb.ugent.be/webtools/Venn/). The affected canonical pathways data retrieved from the IPA analysis of the DEGs were analyzed using hierarchical clustering analysis. Complete linkage and Euclidean distances were employed as metrics to draw association dendrograms between different canonical pathways and the exposure conditions. Cluster analyses and heatmaps were generated using R 3.2.2.[56]

*Statistical Analysis*: Differences between groups were evaluated by one-way ANOVA followed by Dunnet's post hoc test (for comparisons vs control) or by *t*-test (for comparisons between two groups). All analyses were performed using GraphPad Prism 5.02.

*Data Availability*: The transcriptomics data have been deposited in the Gene Expression Omnibus (GEO) (accession number: GSE146482).

## Supporting Information

Supporting Information is available from the Wiley Online Library or from the author.

## Acknowledgements

This work was supported by the European Commission through the GRAPHENE Flagship Project (grant agreement no. 696656). The authors thank the National Genomics Infrastructure (NGI) at Science for Life Laboratory, Stockholm, Sweden, and the Uppsala Multidisciplinary Center for Advanced Computational Science (UPPMAX), Uppsala, Sweden, for assistance with sequencing and for providing the computational infrastructure.

## Conflict of Interest

The authors declare no conflict of interest.

## Author Contributions

S.M. performed the experimental studies and the bioinformatics analyses; G.G. and K.K. contributed to the experimental work and the data analysis; J.W. performed statistical analysis of the sequencing data; A.R. and K.K. (UK) provided GO and physicochemical characterization results; B.F. conceived and supervised the study, analyzed data, and wrote the paper; and all authors approved the final version of the paper.

## Keywords

apoptosis, graphene oxide, lung cells, RNA sequencing, transcriptomics

Received: December 31, 2019
Revised: February 20, 2020
Published online:

[1] B. Fadeel, L. Farcal, B. Hardy, S. Vazquez-Campos, D. Hristozov, A. Marcomini, I. Lynch, E. Valsami-Jones, H. Alenius, K. Savolainen, *Nat. Nanotechnol.* **2018**, *13*, 537.
[2] K. Paunovska, D. Loughrey, C. D. Sago, R. Langer, J. E. Dahlman, *Adv. Mater.* **2019**, *31*, 1902798.
[3] Z. Wang, M. Gerstein, M. Snyder, *Nat. Rev. Genet.* **2009**, *10*, 57.
[4] N. Feliu, P. Kohonen, J. Ji, Y. Zhang, H. L. Karlsson, L. Palmberg, A. Nyström, B. Fadeel, *ACS Nano* **2015**, *9*, 146.
[5] H. D. Mitchell, L. M. Markillie, W. B. Chrisler, M. J. Gaffrey, D. Hu, C. J. Szymanski, Y. Xie, E. S. Melby, A. Dohnalkova, R. C. Taylor, E. K. Grate, S. K. Cooley, J. E. McDermott, A. Heredia-Langner, G. Orr, *ACS Nano* **2016**, *10*, 10173.
[6] J. Bornholdt, A. T. Saber, B. Lilje, M. Boyd, M. Jorgensen, Y. Chen, M. Vitezic, N. R. Jacobsen, S. S. Poulsen, T. Berthing, S. Bressendorff, K. Vitting-Seerup, R. Andersson, K. S. Hougaard, C. L. Yauk, S. Halappanavar, H. Wallin, U. Vogel, A. Sandelin, *ACS Nano* **2017**, *11*, 3597.
[7] M. Mortimer, N. Devarajan, D. Li, P. A. Holden, *ACS Nano* **2018**, *12*, 2728.
[8] B. Fadeel, C. Bussy, S. Merino, E. Vazquez, E. Flahaut, F. Mouchet, L. Evariste, L. Gauthier, A. J. Koivisto, U. Vogel, C. Martin, L. G. Delogu, T. Buerki-Thurnherr, P. Wick, D. Beloin-Saint-Pierre, R. Hischier, M. Pelin, F. Candotto Carniel, M. Tretiach, F. Cesca, F. Benfenati, D. Scaini, L. Ballerini, K. Kostarelos, M. Prato, A. Bianco, *ACS Nano* **2018**, *12*, 10582.
[9] J. Ma, R. Liu, X. Wang, Q. Liu, Y. Chen, R. P. Valle, Y. Y. Zuo, T. Xia, S. Liu, *ACS Nano* **2015**, *9*, 10498.
[10] N. Chatterjee, J. S. Yang, K. Park, S. M. Oh, J. Park, J. Choi, *Environ. Health Toxicol.* **2015**, *30*, e2015007.
[11] S. Mittal, V. Kumar, N. Dhiman, L. K. Chauhan, R. Pasricha, A. K. Pandey, *Sci. Rep.* **2016**, *6*, 39548.
[12] M. Peruzynska, K. Cendrowski, M. Barylak, M. Tkacz, K. Piotrowska, M. Kurzawski, E. Mijowska, M. Drozdzik, *Toxicol. In Vitro* **2017**, *41*, 205.
[13] A. F. Rodrigues, L. Newman, D. A. Jasim, I. A. Vacchi, C. Menard-Moyon, L. E. Crica, A. Bianco, K. Kostarelos, C. Bussy, *Arch. Toxicol.* **2018**, *92*, 3359.
[14] A. F. Rodrigues, L. Newman, N. Lozano, S. P. Mukherjee, B. Fadeel, C. Bussy, K. Kostarelos, *2D Mater.* **2018**, *5*, 035020.
[15] S. P. Mukherjee, K. Kostarelos, B. Fadeel, *Adv. Healthcare Mater.* **2018**, *7*, 1700815.
[16] L. Wang, S. Luanpitpong, V. Castranova, W. Tse, Y. Lu, V. Pongrakhananon, Y. Rojanasakul, *Nano Lett.* **2011**, *11*, 2796.
[17] G. Vales, L. Rubio, R. Marcos, *Nanotoxicology* **2015**, *9*, 568.
[18] W. H. Choo, C. H. Park, S. E. Jung, B. Moon, H. Ahn, J. S. Ryu, K. S. Kim, Y. H. Lee, I. J. Yu, S. M. Oh, *Toxicol. In Vitro* **2016**, *37*, 41.
[19] J. F. Lechner, A. Haugen, I. A. McClendon, E. W. Pettis, *In Vitro* **1982**, *18*, 633.
[20] J. F. Lechner, A. Haugen, I. A. McClendon, A. M. Shamsuddin, *Differentiation* **1984**, *25*, 229.
[21] W. Huber, V. J. Carey, R. Gentleman, S. Anders, M. Carlson, B. S. Carvalho, H. C. Bravo, S. Davis, L. Gatto, T. Girke, R. Gottardo, F. Hahne, K. D. Hansen, R. A. Irizarry, M. Lawrence, M. I. Love, J. MacDonald, V. Obenchain, A. K. Oles, H. Pages, A. Reyes, P. Shannon, G. K. Smyth, D. Tenenbaum, L. Waldron, M. Morgan, *Nat. Methods* **2015**, *12*, 115.

[22] M. D. Robinson, D. J. McCarthy, G. K. Smyth, *Bioinformatics* **2010**, *26*, 139.
[23] A. Krämer, J. Green, J. Pollard, S. Tugendreich, *Bioinformatics* **2014**, *30*, 523.
[24] W. da Huang, B. T. Sherman, R. A. Lempicki, *Nat. Protoc.* **2009**, *4*, 44.
[25] R. Singh, A. Letai, K. Sarosiek, *Nat. Rev. Mol. Cell Biol.* **2019**, *20*, 175.
[26] G. S. Salvesen, C. S. Duckett, *Nat. Rev. Mol. Cell Biol.* **2002**, *3*, 401.
[27] D. W. Nicholson, A. Ali, N. A. Thornberry, J. P. Vaillancourt, C. K. Ding, M. Gallant, Y. Gareau, P. R. Griffin, M. Labelle, Y. A. Lazebnik, N. A. Munday, M. R. Sayyaparaju, M. E. Smulson, T. T. Yamin, V. L. Yu, D. K. Miller, *Nature* **1995**, *376*, 37.
[28] S. Jitkaew, A. Trebinska, E. Grzybowska, G. Carlsson, A. Nordström, J. Lehtiö, A. S. Fröjmark, N. Dahl, B. Fadeel, *J. Biol. Chem.* **2009**, *284*, 27827.
[29] M. Polimeni, G. R. Gulino, E. Gazzano, J. Kopecka, A. Marucco, I. Fenoglio, F. Cesano, L. Campagnolo, A. Magrini, A. Pietroiusti, D. Ghigo, E. Aldieri, *Part. Fibre Toxicol.* **2015**, *13*, 27.
[30] A. R. Gliga, S. Di Bucchianico, J. Lindvall, B. Fadeel, H. L. Karlsson, *Sci. Rep.* **2018**, *8*, 6668.
[31] M. Pelin, L. Fusco, V. Leon, C. Martin, A. Criado, S. Sosa, E. Vazquez, A. Tubaro, M. Prato, *Sci. Rep.* **2017**, *7*, 40572.
[32] M. Pelin, L. Fusco, C. Martin, S. Sosa, J. Frontinan-Rubio, J. M. Gonzalez-Dominguez, M. Duran-Prado, E. Vazquez, M. Prato, A. Tubaro, *Nanoscale* **2018**, *10*, 11820.
[33] N. Chatterjee, H. J. Eom, J. Choi, *Biomaterials* **2014**, *35*, 1109.
[34] Y. Li, Y. Liu, Y. Fu, T. Wei, L. Le Guyader, G. Gao, R. S. Liu, Y. Z. Chang, C. Chen, *Biomaterials* **2012**, *33*, 402.
[35] X. Zhang, Q. Zhou, W. Zou, X. Hu, *Environ. Sci. Technol.* **2017**, *51*, 7861.
[36] A. F. Rodrigues, L. Newman, D. Jasim, S. P. Mukherjee, J. Wang, I. A. Vacchi, C. Ménard-Moyon, A. Bianco, B. Fadeel, K. Kostarelos, C. Bussy, unpublished.
[37] K. E. Wilkinson, L. Palmberg, E. Witasp, M. Kupczyk, N. Feliu, P. Gerde, G. A. Seisenbaeva, B. Fadeel, S. E. Dahlen, V. G. Kessler, *ACS Nano* **2011**, *5*, 5312.
[38] P. M. Costa, B. Fadeel, *Toxicol. Appl. Pharmacol.* **2016**, *299*, 101.
[39] F. T. Andon, B. Fadeel, *Acc. Chem. Res.* **2013**, *46*, 733.
[40] B. Fadeel, B. Zhivotovsky, S. Orrenius, *FASEB J.* **1999**, *13*, 1647.
[41] X. B. Qiu, S. L. Markant, J. Yuan, A. L. Goldberg, *EMBO J.* **2004**, *23*, 800.
[42] T. Bartke, C. Pohl, G. Pyrowolakis, S. Jentsch, *Mol. Cell* **2004**, *14*, 801.
[43] P. Ebner, I. Poetsch, L. Deszcz, T. Hoffmann, J. Zuber, F. Ikeda, *Nat. Commun.* **2018**, *9*, 599.
[44] Y. Hao, K. Sekine, A. Kawabata, H. Nakamura, T. Ishioka, H. Ohata, R. Katayama, C. Hashimoto, X. Zhang, T. Noda, T. Tsuruo, M. Naito, *Nat. Cell Biol.* **2004**, *6*, 849.
[45] F. Li, Q. Huang, J. Chen, Y. Peng, D. R. Roop, J. S. Bedford, C. Y. Li, *Sci. Signaling* **2010**, *3*, ra13.
[46] C. Nakahashi-Oda, K. G. Udayanga, Y. Nakamura, Y. Nakazawa, N. Totsuka, H. Miki, S. Iino, S. Tahara-Hanaoka, S. Honda, K. Shibuya, A. Shibuya, *Nat. Immunol.* **2016**, *17*, 441.
[47] C. E. Fogarty, A. Bergmann, *Curr. Top. Dev. Biol.* **2015**, *114*, 241.
[48] S. P. Mukherjee, N. Lozano, M. Kucki, A. E. Del Rio-Castillo, L. Newman, E. Vazquez, K. Kostarelos, P. Wick, B. Fadeel, *PLoS One* **2016**, *11*, e0166816.
[49] A. Gallud, K. Klöditz, J. Ytterberg, N. Östberg, S. Katayama, T. Skoog, V. Gogvadze, Y. Z. Chen, D. Xue, S. Moya, J. Ruiz, D. Astruc, R. Zubarev, J. Kere, B. Fadeel, *Sci. Rep.* **2019**, *9*, 4366.
[50] A. Dobin, C. A. Davis, F. Schlesinger, J. Drenkow, C. Zaleski, S. Jha, P. Batut, M. Chaisson, T. R. Gingeras, *Bioinformatics* **2013**, *29*, 15.
[51] Y. Liao, G. K. Smyth, W. Shi, *Bioinformatics* **2014**, *30*, 923.
[52] M. Pertea, G. M. Pertea, C. M. Antonescu, T. C. Chang, J. T. Mendell, S. L. Salzberg, *Nat. Biotechnol.* **2015**, *33*, 290.
[53] L. Wang, S. Wang, W. Li, *Bioinformatics* **2012**, *28*, 2184.
[54] S. Sayols, D. Scherzinger, H. Klein, *BMC Bioinformatics.* **2016**, *17*, 428.
[55] A. R. Gliga, K. Edoff, F. Caputo, T. Källman, H. Blom, H. L. Karlsson, L. Ghibelli, E. Traversa, S. Ceccatelli, B. Fadeel, *Sci. Rep.* **2017**, *7*, 9284.
[56] R. Ihaka, R. Gentleman, *J. Comput. Graph. Stat.* **1996**, *5*, 299.